VIP Light Harvesting Very Important Paper

Deutsche Ausgabe: DOI: 10.1002/ange.201600279
Internationale Ausgabe: DOI: 10.1002/anie.201600279

Flexible Near-Infrared Photovoltaic Devices Based on Plasmonic Hot-Electron Injection into Silicon Nanowire Arrays

*Dong Liu[+], Dong Yang[+], Yang Gao, Jun Ma, Ran Long, Chengming Wang, and Yujie Xiong**

Abstract: *The development of flexible near-infrared (NIR) photovoltaic (PV) devices containing silicon meets the strong demands for solar utilization, portability, and sustainable manufacture; however, improvements in the NIR light absorption and conversion efficiencies in ultrathin crystalline Si are required. We have developed an approach to improve the quantum efficiency of flexible PV devices in the NIR spectral region by integrating Si nanowire arrays with plasmonic Ag nanoplates. The Ag nanoplates can directly harvest and convert NIR light into plasmonic hot electrons for injection into Si, while the Si nanowire arrays offer light trapping. Taking the wavelength of 800 nm as an example, the external quantum efficiency has been improved by 59% by the integration Ag nanoplates. This work provides an alternative strategy for the design and fabrication of flexible NIR PVs.*

Photovoltaic (PV) technologies that harvest and convert sunlight directly into electricity will play a vital role in efforts to provide clean and secure sources of energy. To fully utilize solar energy, near-infrared (NIR) light ($780 < \lambda < 2500$ nm) which accounts for about 52% of solar photons should be harvested for electricity generation. As most of the existing PV devices are designed for visible-light utilization, there is a strong demand to develop NIR PV modules through device structure and mechanism innovation. Toward sustainable development, the PV device manufacture eventually requires low-cost, high-abundance materials, and an environmentally friendly fabrication process.[1,2] Silicon is the second most abundant element in the earth's crust and is a widely utilized material in semiconductor technology with a high level of ease in manufacturing. This nontoxic semiconductor can absorb photons at energies above 1.1 eV,[3,4] providing a possibility for harvesting the NIR light at $\lambda < 1100$ nm; however, its quantum efficiency for NIR photon conversion is not as high as that for visible light.

[*] D. Liu,[+] D. Yang,[+] Y. Gao, J. Ma, Dr. R. Long, Dr. C. Wang, Prof. Y. Xiong
Hefei National Laboratory for Physical Sciences at the Microscale
*i*ChEM (Collaborative Innovation Center of Chemistry for Energy Materials), Hefei Science Center (CAS)
School of Chemistry and Materials Science, and USTC Center for Micro- and Nanoscale Research and Fabrication
University of Science and Technology of China
Hefei, Anhui 230026 (P. R. China)
E-mail: yjxiong@ustc.edu.cn

[+] These authors contributed equally to this work.

Supporting information for this article (including device fabrication and characterization methods) can be found under http://dx.doi.org/10.1002/anie.201600279.

In addition to NIR applications, another major trend in PV development is to fabricate lightweight devices with mechanical flexibility.[5] To this end, very thin layers of absorber materials (e.g., ultrathin crystalline Si) are used in PV cells.[6] The reduction in Si absorber thickness greatly compromises the light absorption of devices, particularly in the NIR spectral region.[7,8] To efficiently harvest or trap the light, semiconductor nanostructures (e.g., nanowire arrays),[9,10] absorber materials with multiple energy bands,[11,12] and surface plasmonic elements for subwavelength scattering[8,13–15] have been designed and used in PV devices. Light harvesting by nanowire arrays and plasmonic scattering, in which multiple reflection increases light traveling path lengths, has been validated for various types of solar cells including p–n junctions,[3,10] inorganic–organic hybrids,[9,16–18] and Schottky-type devices.[19–21] According to the established mechanisms, apparently such light trapping only works for the spectral range where the photons can be effectively absorbed and converted by semiconductor. As the use of crystalline Si cannot result in large absorption coefficients and high conversion efficiencies for NIR light,[7] the NIR improvement on Si-based PVs by light-trapping techniques would be limited.

Herein, we demonstrate the fabrication of flexible PV cells with the improved NIR efficiency in the NIR region through the implementation of plasmonic hot-electron injection into monocrystalline Si nanowire arrays (Si NWs). The generation of hot electrons in metal nanostructures is a nonradiative process that occurs parallel to radiative scattering during plasmon decay.[22,23] The excited hot electrons occupy high energy levels so as to overcome the Schottky barrier and flow into the conduction band of semiconductor when the metal forms a Schottky junction with an n-type semiconductor.[24–27] If this electron flow can synergize with the carrier migration in PV cells, it would offer improved efficiency for electricity generation. As such, it no longer relies on the capability of Si in photon harvesting and conversion.

We first demonstrated our concept based on inorganic–organic hybrid Si-poly(3,4-ethylenedioxythiophene)/poly-(styrene sulfonate) (PEDOT:PSS) PV cells. To prove the concept that NIR plasmonic nanostructures can inject hot electrons into PV devices, the devices fabricated from conventional 400 μm thick Si wafers were firstly used as model systems for analyses. As illustrated in Figure 1a, we first fabricated monocrystalline n-type Si nanowire arrays from n-type Si wafers by metal-assisted etching.[28–30] As a result, the nanowire arrays were supported on the wafers, thus providing a platform for further device fabrication. The nanowire arrays allow trapping of the light that can be effectively absorbed by crystalline Si.

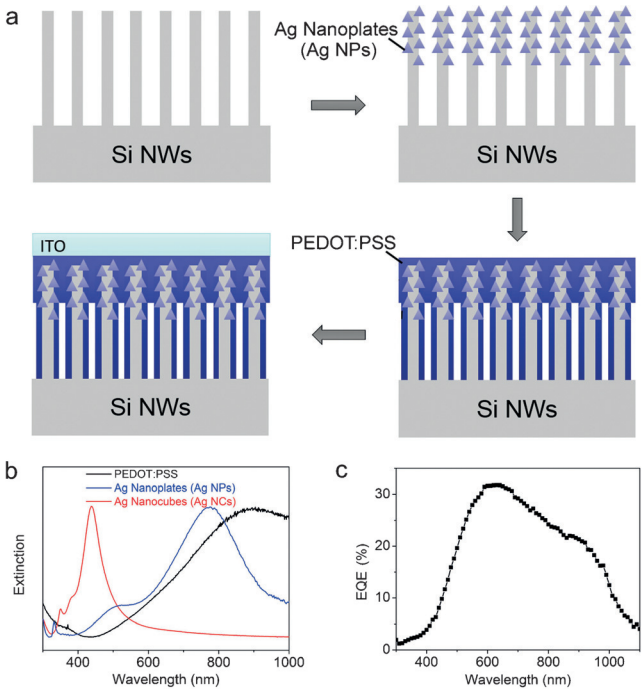

Figure 1. a) Fabrication process for a Si NWs/Ag NPs/PEDOT:PSS hybrid photovoltaic device: formation of Si nanowire arrays (Si NWs) by wet etching, dropcasting of Ag nanoplates (Ag NPs) on the sidewalls of Si NWs, coating of PEDOT:PSS, and packaging with ITO. b) Normalized UV/Vis spectra of Ag nanocubes and nanoplates suspended in water and PEDOT:PSS dissolved in ethanol. c) EQE plots of the n-type Si NWs/PEDOT:PSS device (fabricated from 400 μm thick Si wafer) from IPCE measurements.

An suspension of Ag nanostructures in ethanol was then dropcast into the Si nanowire arrays (see Figure S1 in the Supporting Information). We selected Ag nanostructures as plasmonic elements owing to their appropriate work function for the establishment of Schottky junctions with n-type Si, as well as their tunable plasmonic bands that can be altered by tailoring the shapes of the Ag species, namely nanocubes (NCs) and nanoplates (NPs; see images in Figure S2). As shown in UV/Vis extinction spectra (Figure 1b), the Ag nanoplates and nanocubes exhibit plasmonic bands covering 550–1100 nm and 350–550 nm, respectively. Intuitively, the broad plasmonic band of Ag nanoplates should make them excellent candidates for hot-electron injection to enhance NIR quantum efficiency.

In the next step, an ethanolic solution containing PEDOT:PSS was coated onto the sample. The PEDOT:PSS is a hole-transporting agent that absorbs light in the NIR region (Figure 1b), which can readily penetrate into the nanowire arrays. As a final step, the device was covered by a front electrode comprising PEDOT:PSS-coated indium tin oxide (ITO) glass, and an Ag back electrode was formed on the back side of the Si wafer.

We first analyzed the performance of inorganic–organic n-Si NWs/PEDOT:PSS junction in the absence of Ag nanostructures (see images in Figure S1). As indicated by incident-photon-to-current conversion efficiency (IPCE) measurements (Figure 1c), the external quantum efficiency (EQE) of n-Si NWs/PEDOT:PSS reaches the maximum of 31.8% at 630 nm. In this device configuration, the direct junction between n-type Si nanowires and PEDOT:PSS can work as a photovoltaic cell (Figure 2a) according to previous studies.[17,31] Under illumination, the electrons in the n-type Si nanowires are photoexcited from the valence to the conduction bands. As the lowest unoccupied molecular orbital (LUMO) level of the hole-transporting agent PEDOT:PSS is relatively high, the photoexcited electrons in Si cannot overcome the bending barrier of Si close to PEDOT:PSS. Instead, the electrons would flow in one direction to the back metal contact. In the meantime, the photogenerated holes can by transported via the occupied molecular orbital of PEDOT:PSS and be collected by the front ITO glass contact.

When Ag nanostructures are integrated between Si nanowires and PEDOT:PSS (Figure 2b), the plasmonic hot electrons generated from Ag by illumination can be injected into the conduction band of n-type Si by overcoming or tunneling through the band bending (i.e., the Schottky barrier between n-Si and Ag).[26,32] The plasmonic holes in Ag would be incorporated in the hole-transport flow toward the ITO glass contact. It is anticipated that the Ag nanoplates generating hot electrons at 550–1100 nm can enhance PV performance in the NIR region. Figure 2c shows the *J*–*V* characteristics of the n-type Si NWs/PEDOT:PSS with or without Ag nanoplates (i.e., Si NWs/Ag NPs/PEDOT:PSS and Si NWs/PEDOT:PSS, respectively) taken under AM1.5

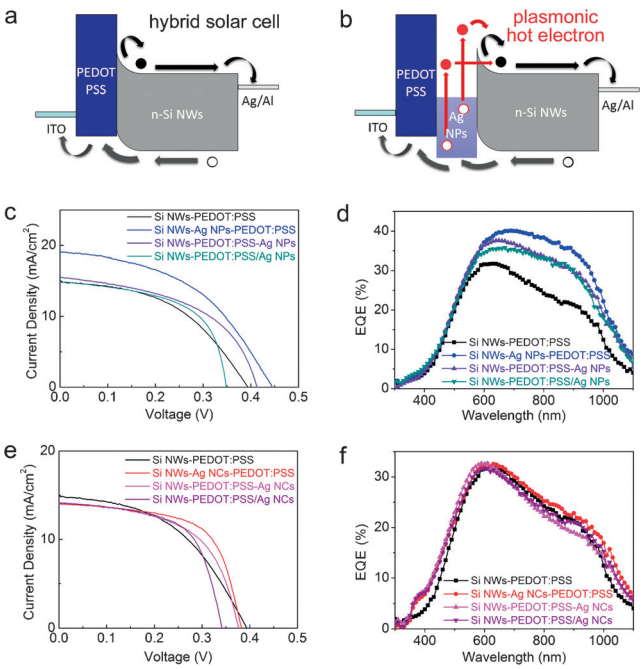

Figure 2. Energy diagrams and carrier migration schematics for a) n-Si NWs/PEDOT:PSS and b) n-Si NWs/Ag NPs/PEDOT:PSS devices. The black dots and circles represent the photoexcited electrons and holes in PV devices, respectively, and the red dots denote the plasmonic hot electrons generated from Ag nanoplates. c) Current density-voltage (*J*–*V*) curves and d) EQE plots of the n-Si NWs/PEDOT:PSS devices with or without Ag nanoplates. e) *J*–*V* curves and f) EQE plots of the n-Si NWs/PEDOT:PSS devices with or without Ag nanocubes, fabricated from 400 μm thick Si wafers.

illumination. To elucidate the importance of hot electron injection into Si, we have compared the performance of Si NWs/Ag NPs/PEDOT:PSS with two reference samples: Si NWs/PEDOT:PSS/Ag NPs (coating of PEDOT:PSS on Si followed by dropcast of Ag nanoplates) and Si NWs/PEDOT:PSS/Ag NPs (dropcast of mixture of PEDOT:PSS and Ag nanoplates on Si). As indicated by the photovoltaic parameters summarized in Table S1, the direct contact of Ag nanoplates with n-type Si nanowires can effectively improve the performance, achieving dramatically higher efficiency than the other configurations. The current density and power conversion efficiency are increased by 28% and 40%, respectively when the Ag nanoplates are in contact with the Si nanowires in the devices.

The role of the Ag nanoplates can be better understood by studying plots of EQE versus wavelength. As shown in Figure 2d, the quantum efficiencies were substantially enhanced by the Si NWs/Ag NPs junction at 550–1100 nm, which matches well with the plasmonic band of the Ag nanoplates. As a result, the maximum EQE has achieved 40.0%, and the EQEs are maintained above 30.0% in a broad spectral range of 550–960 nm. As compared with the Si NWs/PEDOT:PSS junction, the maximum wavelength was shifted from 630 nm to 680 nm toward the absorption maxima of plasmonic Ag nanoplates at 800 nm. Taking the wavelength of absorption maxima as an example, the EQE has been improved from 24.2% to 38.4% with 59% enhancement by use of the Ag nanoplates. In comparison, when the Ag nanocubes with the same Fermi level were used, the power conversion efficiency could only be enhanced by 7% (see Figure 2e and Table S2). The EQE measurements (Figure 2f) show that the enhancement mainly takes place at 350–550 nm, which overlaps with the plasmonic band of the Ag nanocubes. As crystalline Si typically possesses a high conversion efficiency for visible light, the enhancement factor by Ag nanocubes is very limited.

To confirm that the plasmonic enhancement works through hot electrons rather than scattering, we have performed studies on p-type Si nanowires. The injection of plasmonic hot carriers relies on band structures, whereas the effect from plasmonic scattering should work for all the device configurations.[32] In the case of p-type Si nanowires (Figure S3), it will form a potential well at the contact zone with PEDOT:PSS. The photoexcited electrons in p-type Si would flow into the well and try to cross the LUMO level of PEDOT:PSS. The unfavorable migration of electrons toward the typical hole-transporting agent results in the very small current and low conversion efficiency as shown in Figure S4 and Table S3. As Ag nanoplates are integrated between p-Si and PEDOT:PSS, plasmonic hot holes can be injected into the valence band of p-Si; however, the photoexcited electrons in p-Si would fall into the well for charge recombination (see Figure S3), thus reducing the conversion efficiency. This behavior indicates that plasmonic scattering has little effect on the device performance enhancement.

The strategy of employing plasmonic hot electrons for enhancing NIR PV performance can be extended to another type of device such as Schottky-type solar cells comprising n-type Si nanowire arrays and reduced graphene oxide (rGO). As illustrated in Figure 3a, a Schottky barrier would be formed when rGO comes into contact with n-type Si.[20,21] The photoexcited electrons in Si are repelled by the Schottky barrier, while the holes migrate toward rGO. When Ag nanoplates are inserted into the junction (Figure 3b), the plasmonic hot electrons can enter the conduction band of n-type Si, similar to the behavior in the n-Si NWs/Ag NPs/PEDOT:PSS. As indicated by *J*–*V* (Figure 4c) and EQE (Figure 4d) measurements, the hot-electron injection significantly improves the PV efficiency in the plasmonic band of Ag nanoplates, with enhancements of about six times for current

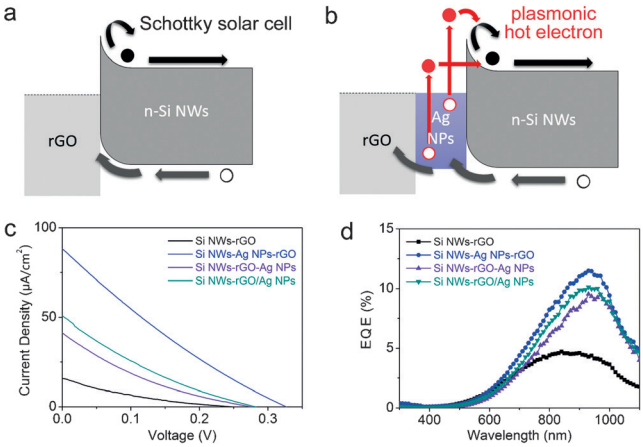

Figure 3. Energy diagrams and carrier migration schematics for a) n-Si NWs/rGO and b) n-Si NWs/Ag NPs/rGO devices. The black dots and circles represent the photoexcited electrons and holes in PV devices, respectively, and the red dots denote the plasmonic hot electrons generated from Ag nanoplates. c) *J*–*V* curves and d) EQE plots of the n-Si NWs/rGO devices with or without Ag nanoplates, fabricated from 400 μm thick Si wafers.

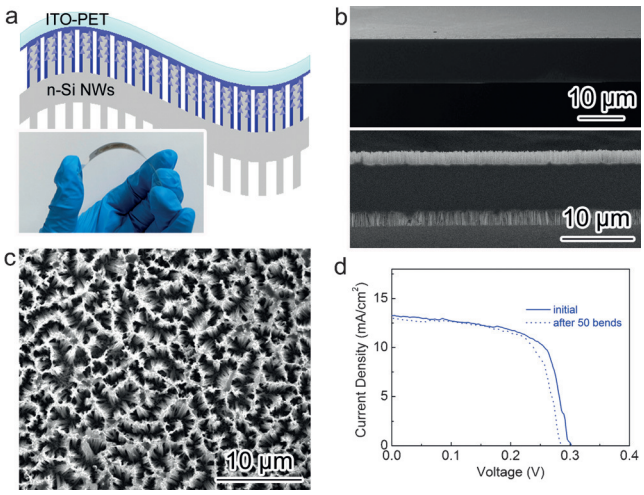

Figure 4. a) Structure of flexible n-Si NWs/Ag NPs/PEDOT:PSS device, fabricated from 10 μm thick Si film. The inset shows the photograph of a flexible device. b) Side-view SEM images of the Si ultrathin wafer (top panel) and nanowire arrays (bottom panel) used for fabrication. c) Top-view SEM image of the Si nanowire arrays. d) *J*–*V* curves of a flexible n-Si NWs/PEDOT:PSS device before and after 50 bends.

density and eight times for power conversion efficiency. Similar to the n-Si NWs/Ag NPs/PEDOT:PSS devices, the switch of n-type to p-type Si nanowire arrays suppresses the PV conversion of n-Si NWs/Ag NPs/rGO (see Figure S5 and Figure S6). We can thus conclude that the injection of plasmonic hot electrons indeed enhances the photon harvesting and conversion in PV devices.

After elucidating the role of plasmonic nanostructures, we were in a position to implement our design in flexible n-Si NWs/Ag NPs/PEDOT:PSS PV devices (Figure 4a). To fabricate large-area devices, we have employed inductively coupled plasma–reactive ion etching (ICP-RIE) to uniformly thin the mother Si wafers. The thickness of the ultrathin Si wafers can be highly controlled, and the RIE-etched wafers are very smooth, as indicated by the cross-section SEM image (top panel of Figure 4b). For the fabrication of flexible devices (Figure 4a, inset), we thinned the wafer down to 10 μm. After three minutes of metal-assisted wet etching, n-type Si nanowire arrays were fabricated on the double sides of the wafer (see SEM images in the bottom panel of Figure 4b and Figure 4c). Such a double-sided nanowire array configuration enables the mechanical flexibility of Si film over a relatively large area (1.5×1.5 cm^2). Further device fabrication was conducted by following the same procedure as that for conventional Si wafer, except for the use of flexible ITO-polyethylene terephthalate (PET) plastic film as the front electrode. The obtained flexible device exhibited excellent performance durability in a bending test (Figure 4d). Note that the open-circuit voltage (V_{oc}) and short-circuit current (J_{sc}) of this device are relatively lower as compared with the bulk one mentioned above because of the larger resistance of ITO-PET (30 Ω/sq versus 8 Ω/sq for ITO glass) and worse edge contact of PEDOT:PSS with the large-area ultrathin Si film.[33] It is believed that a future modification on device structure and electrode material will boost the PV performance.

In summary, we have developed an approach to integrate plasmonic hot electron injection into Si nanowire arrays for enhanced PV performance in the NIR spectral region, based on two different types of PV devices. Taking the wavelength of 800 nm as an example, the use of Ag nanoplates has resulted in a 59% enhancement of the EQE from 24.2% to 38.4%. This strategy has enabled the fabrication of NIR PV devices with mechanical flexibility. The concept demonstrated here should be easily extended to the fabrication of other flexible PV devices, with further modifications on device structures and fabrication techniques, to achieve the further boosted power conversion efficiency. Thus this work presents an alternative strategy for the design and fabrication of flexible NIR PVs, and provides insights into the utilization of surface-plasmonic-induced hot electrons for other areas that involve solar energy conversion.

Acknowledgements

This work was financially supported by the NSFC (No. 91123010, 21471141), the Specialized Research Fund for the Doctoral Program of Higher Education (No. 20123402110050), the Recruitment Program of Global Experts, the CAS Hundred Talent Program, the Hefei Science Center CAS (2015HSC-UP009), and the Fundamental Research Funds for the Central Universities (Nos. WK2060190025 and WK2310000035). This work was partially carried out at the USTC Center for Micro and Nanoscale Research and Fabrication.

Keywords: flexible devices · hot electrons · photovoltaics · plasmonics · silicon

How to cite: *Angew. Chem. Int. Ed.* **2016**, *55*, 4577–4581
Angew. Chem. **2016**, *128*, 4653–4657

[1] J. Jean, P. R. Brown, R. L. Jaffe, T. Buonassisi, V. Bulović, *Energy Environ. Sci.* **2015**, *8*, 1200.
[2] J. Oh, H. C. Yuan, H. M. Branz, *Nat. Nanotechnol.* **2012**, *7*, 743.
[3] V. Sivakov, G. Andra, A. Gawlik, A. Berger, J. Plentz, F. Falk, S. H. Christiansen, *Nano Lett.* **2009**, *9*, 1549.
[4] D. Liu, L. Li, Y. Gao, C. Wang, J. Jiang, Y. Xiong, *Angew. Chem. Int. Ed.* **2015**, *54*, 2980; *Angew. Chem.* **2015**, *127*, 3023.
[5] J. Yoon, A. J. Baca, S. I. Park, P. Elvikis, J. B. Geddes III, L. Li, R. H. Kim, J. Xiao, S. Wang, T. H. Kim, M. J. Motala, B. Y. Ahn, E. B. Duoss, J. A. Lewis, R. G. Nuzzo, P. M. Ferreira, Y. Huang, A. Rockett, J. A. Rogers, *Nat. Mater.* **2008**, *7*, 907.
[6] S. Pan, Z. Yang, P. Chen, J. Deng, H. Li, H. Peng, *Angew. Chem. Int. Ed.* **2014**, *53*, 6110; *Angew. Chem.* **2014**, *126*, 6224.
[7] J. Nelson, *The Physics of Solar Cells*, Imperial College Press, London, UK, **2003**.
[8] H. A. Atwater, A. Polman, *Nat. Mater.* **2010**, *9*, 205.
[9] X. Shen, B. Sun, D. Liu, S. T. Lee, *J. Am. Chem. Soc.* **2011**, *133*, 19408.
[10] E. Garnett, P. Yang, *Nano Lett.* **2010**, *10*, 1082.
[11] J. Yang, J. B. You, C. C. Chen, W. C. Hsu, H. R. Tan, X. W. Zhang, Z. R. Hong, Y. Yang, *ACS Nano* **2011**, *5*, 6210.
[12] B. Niesen, N. Blondiaux, M. Boccard, M. Stuckelberger, R. Pugin, E. Scolan, F. Meillaud, F. J. Haug, A. Hessler-Wyser, C. Ballif, *Nano Lett.* **2014**, *14*, 5085.
[13] S. W. Baek, G. Park, J. Noh, C. Cho, C. H. Lee, M. K. Seo, H. Song, J. Y. Lee, *ACS Nano* **2014**, *8*, 3302.
[14] P. Reineck, G. P. Lee, D. Brick, M. Karg, P. Mulvaney, U. Bach, *Adv. Mater.* **2012**, *24*, 4750.
[15] D. M. Schaadt, B. Feng, E. T. Yu, *Appl. Phys. Lett.* **2005**, *86*, 063106.
[16] J. He, P. Q. Gao, M. D. Liao, X. Yang, Z. Q. Ying, S. Q. Zhou, J. C. Ye, Y. Cui, *ACS Nano* **2015**, *9*, 6522.
[17] S. Thiyagu, C. C. Hsueh, C. T. Liu, H. J. Syu, T. C. Lin, C. F. Lin, *Nanoscale* **2014**, *6*, 3361.
[18] S. Li, Z. Pei, F. Zhou, Y. Liu, H. Hu, S. Ji, C. Ye, *Nano Res.* **2015**, *8*, 3141.
[19] G. Fan, H. Zhu, K. Wang, J. Wei, X. Li, Q. Shu, N. Guo, D. Wu, *ACS Appl. Mater. Interfaces* **2011**, *3*, 721.
[20] X. Li, H. Zhu, K. Wang, A. Cao, J. Wei, C. Li, Y. Jia, Z. Li, X. Li, D. Wu, *Adv. Mater.* **2010**, *22*, 2743.
[21] C. Xie, P. Lv, B. Nie, J. Jie, X. Zhang, Z. Wang, P. Jiang, Z. Hu, L. Luo, Z. Zhu, L. Wang, C. Wu, *Appl. Phys. Lett.* **2011**, *99*, 133113.
[22] S. Linic, U. Aslam, C. Boerigter, M. Morabito, *Nat. Mater.* **2015**, *14*, 567.
[23] G. V. Hartland, *Chem. Rev.* **2011**, *111*, 3858.
[24] M. L. Brongersma, N. J. Halas, P. Nordlander, *Nat. Nanotechnol.* **2015**, *10*, 25.
[25] C. Clavero, *Nat. Photonics* **2014**, *8*, 95.
[26] M. W. Knight, H. Sobhani, P. Nordlander, N. J. Halas, *Science* **2011**, *332*, 702.
[27] F. B. Atar, E. Battal, L. E. Aygun, B. Daglar, M. Bayindir, A. K. Okyay, *Opt. Express* **2013**, *21*, 7196.

[28] M. L. Zhang, K. Q. Peng, X. Fan, J. S. Jie, R. Q. Zhang, S. T. Lee, N. B. Wong, *J. Phys. Chem. C* **2008**, *112*, 4444.
[29] K. Q. Peng, Y. Wu, H. Fang, X. Y. Zhong, Y. Xu, J. Zhu, *Angew. Chem. Int. Ed.* **2005**, *44*, 2737; *Angew. Chem.* **2005**, *117*, 2797.
[30] Z. Huang, X. Zhang, M. Reiche, L. Liu, W. Lee, T. Shimizu, S. Senz, U. Gosele, *Nano Lett.* **2008**, *8*, 3046.
[31] S. Smith, S. R. Forrest, *Appl. Phys. Lett.* **2004**, *84*, 5019.
[32] A. O. Govorov, H. Zhang, Y. K. Gun′ko, *J. Phys. Chem. C* **2013**, *117*, 16616.
[33] W. J. Potscavage, A. Sharma, B. Kippelen, *Acc. Chem. Res.* **2009**, *42*, 1758.

Received: January 10, 2016
Published online: March 1, 2016

